Electronic, Rovibrational, and Translational Energy Effects in Ion−Alkylbenzene Charge-Transfer Reactions†

Skip Williams,* Anthony J. Midey, Susan T. Arnold, Robert A. Morris, Albert A. Viggiano, Yu-Hui Chiu,‡ Dale J. Levandier,‡ and Rainer A. Dressler

Air Force Research Laboratory, Space Vehicles Directorate, 29 Randolph Road, Hanscom AFB, Massachusetts 01731-3010

Michael R. Berman

Air Force Office of Scientific Research, Chemistry and Life Sciences Directorate, 801 N. Randolph St., Arlington, Virginia 22203-1977

Received: April 14, 2000; In Final Form: June 21, 2000

Rate constants and branching fractions are reported for the reactions of NO^+, Xe_2^+, O_2^+, $Xe^+(^2P_{3/2})$, and $Kr^+(^2P_{3/2})$ with toluene, ethylbenzene, and *n*-propylbenzene. Ions with recombination energies ranging from 9.26 eV (NO^+) to 14.00 eV (Kr^+) are studied at 300 K in a variable temperature−selected ion flow tube (VT-SIFT) yielding information regarding the role of electronic energy in these reactions. The reactions of NO^+ and O_2^+ have been studied between 300 and 500 K in the VT-SIFT and between 500 and 1400 K in a high-temperature flowing afterglow (HTFA) apparatus to investigate the role of rovibrational energy. The effect of translational energy in these reactions has been investigated with a guided-ion beam (GIB) apparatus using a high-temperature octopole (HT8P) operating under single collision conditions. In the GIB-HT8P experiments, the center-of-mass collision energy was varied from ca. 0.1 to 7 eV for reactions of NO^+ and O_2^+, and the target gas temperature was varied between 300 and 800 K. All reactions are found to proceed near the capture rate at all temperatures studied. The reactions proceed primarily by nondissociative and dissociative charge transfer except for the reaction involving NO^+, where the dissociation products observed in the HTFA experiments at high temperature are attributed to thermal decomposition of the charge-transfer product ions. Generally, electronic and vibrational energy are both very effective in promoting dissociation while translational energy is found to be less effective.

I. Introduction

Several researchers have pointed out that a fundamental understanding of detailed combustion chemistry is necessary for the development of hydrocarbon fueled advanced air-breathing propulsion systems.[1−3] The rocket-based combined cycle (RBCC) engine being developed for Earth-to-orbit reusable launch vehicles which integrates an air-augmented rocket, a ramjet, and a supersonic ramjet (scramjet) into a single system is a notable example.[4] Airbreathing propulsion at RBCC velocities is subject to the stressing requirement that ignition and combustion must take place on very rapid time scales since combustors feature millisecond residence times commensurate with combustion reaction time scales (1 μs to 10 ms). Previous efforts have established the effectiveness of utilizing high-temperature plasma jets to cause ignition and rapid flame propagation in hydrocarbon−air mixtures.[5,6] Renewed interest in the development of high-speed airbreathing propulsion technology[7] has prompted a number of investigators to consider adopting plasmas as ignition aids in scramjet combustors with positive results.[8−10]

On the other hand, computational studies attempting to assess the importance of ionic mechanisms in combustion have been impeded by a lack of kinetic data at relevant temperatures.[11] Historically, ionization and recombination processes at high temperatures have been studied in flames and shock tubes dating back many years.[12,13] However, the study of individual ion−molecule reactions under controlled conditions has been mainly at or near room temperature.[14] There have been only two studies outside our laboratories where rate constants and branching fractions have been measured above 600 K,[15,16] and such data above 900 K is essentially nonexistent. High-temperature kinetics data are required because extrapolation of low-temperature data is often unreliable.[17] In order to circumvent these and other problems, the Air Force Research Laboratory has developed two high-temperature apparatuses capable of studying individual ion−molecule reactions: a high-temperature flowing afterglow apparatus[18] capable of measuring thermal ion−molecule reaction rate constants and branching fractions up to 1800 K at a pressure of approximately 1 Torr; and a high-temperature guided-ion beam apparatus[19] capable of measuring ion−molecule reaction cross sections and branching fractions up to 1100 K under single collision conditions.

Recently, numerous air plasma ion reactions with hydrocarbons at high temperature have been investigated, and these data are being compiled for use in computational modeling studies regarding the effects of ionization in combustion. Reactions of various atmospheric plasma ions (NO^+, N_2^+, O_2^+, O^+, N^+, H_3O^+) with aliphatic hydrocarbons have been studied previously

† Part of the special issue "C. Bradley Moore Festschrift".

‡ Under contract to Institute of Scientific Research, Boston College, Newton, MA 02159.

* Corresponding author.

10.1021/jp001428n CCC: $19.00
Published on Web 09/07/2000

as a function of temperature using flow tube methods.[20−22] Incorporating these ionic mechanisms into detailed hydrocarbon combustion kinetics models demonstrates that ionization speeds the rate of combustion.[23,24] In order to expand the database of ion chemistry available for the combustion kinetics and soot formation models, a study of atmospheric plasma ions reacting with aromatic hydrocarbons has been undertaken.[25−27] Most liquid hydrocarbon aviation and rocket fuels are mixtures of a large number of hydrocarbons that contain as much as 25 vol % aromatics of which alkylbenzenes figure predominately. Therefore, high-temperature rate constants and branching fractions are being studied for the reactions of several ions with various alkylbenzene reactants.

The construction of product ion breakdown diagrams has proved to be a valuable method for characterizing charge-transfer reactions involving aromatic reactants.[25,26] A breakdown diagram for a particular reactant consists of plotting the parent and various product ion branching fractions as a function of total available energy. The average total energy, $\langle \bar{E}_{\text{total}} \rangle$, available for reaction at temperature T is defined as

$$\langle \bar{E}_{\text{total}} \rangle = \text{RE}_{\text{ion}} + \langle E_{\text{trans}} \rangle + \langle E_{\text{rot}}^{\text{aromatic}} \rangle + \langle E_{\text{vib}}^{\text{aromatic}} \rangle + \langle E_{\text{in}}^{\text{ion}} \rangle \quad (1)$$

In eq 1, RE_{ion} is the recombination energy of the reactant ion which for most ions is simply the ionization energy of the neutral precursor. However, if the ground electronic state of the neutral precursor is repulsive, the recombination energy corresponds to the vertical recombination energy to the repulsive region of the neutral potential. The other terms appearing in eq 1 are defined as follows. The average translational energy, $\langle E_{\text{trans}} \rangle$, is $^3/_2 k_B T$ in flow tube experiments and is the nominal CM collision energy in drift tube and guided-ion beam experiments. The average rotational energy of the aromatic reactant, $\langle E_{\text{rot}}^{\text{aromatic}} \rangle$, is $^3/_2 k_B T$, the average aromatic reactant vibrational energy, $\langle E_{\text{vib}}^{\text{aromatic}} \rangle$, is an ensemble average over a Boltzmann distribution of vibrational energy levels for the $3N - 6$ modes, and $\langle E_{\text{in}}^{\text{ion}} \rangle$ is the corresponding average reactant ion internal energy.

The efficacy of certain types of energy in promoting a particular reaction channel can be readily evaluated by comparing the breakdown curves for different experiments. For instance, varying the recombination energy of the primary ion, as is done in this paper, yields information regarding the role of electronic energy in these reactions as pointed out by Ausloos.[28] This statement follows from charge-transfer energy resonance criteria where the charge-transfer probability can be described as the product between the pure electronic coupling and the Franck−Condon overlap between reactant and product wave functions.[29] The excellent agreement between breakdown curves for benzene[25] and naphthalene[26] obtained using thermal charge-transfer mass spectrometry and photoexcitation confirms the important role of energy resonance in these aromatic systems. Furthermore, aromatic molecules, such as the alkylbenzenes studied here, are capable of "storing" significant amounts of rovibrational energy at high temperatures because these molecules contain a large number of low to moderate frequency vibrational modes. Thus, varying the temperature of the experiment increases the rovibrational energy available for reaction. The translational energy of ion−molecule reactions is varied simply by accelerating the primary reactant ion in an electric field.

Reactions of toluene (C_7H_8), ethylbenzene (C_8H_{10}), and *n*-propylbenzene (C_9H_{12}) with ions having recombination energies ranging from 9.26 eV (NO^+) to 14.00 eV (Kr^+) have been measured at 300 K to study the role of electronic energy. Data for the reactions of NO^+ and O_2^+ with these alkylbenzenes have been measured between 300 and 1400 K to investigate the role of rovibrational energy. In addition, the effect of translational energy in these reactions has been investigated over center-of-mass (CM) collision energies ranging from ca. 0.1 to 7 eV for reactions of NO^+ and O_2^+ between 300 and 800 K. The observed reaction rate constants and product branching fractions are presented within the context of previous work and the implications for detailed kinetic modeling applications are discussed.

II. Experiment

The plasma chemistry of ionized air reacting with hydrocarbons is investigated using fast ion flow tube kinetics and guided-ion beam instrumentation. The variable temperature−selected ion flow tube (VT-SIFT) instrument can be used to measure both reaction rate constants and branching fractions as a function of temperature from 80 to 550 K. Measurements at higher temperatures are conducted using a second fast flow tube instrument, the high-temperature flowing afterglow (HTFA). The HTFA provides data from 300 to 1800 K (±2% accuracy) enabling the study of ion−molecule reactions at temperatures relevant to plasma and combustion chemistry. Both instruments operate at ca. 1 Torr of helium buffer pressure, and the kinetics are observed over ca. 1−4 ms reaction time. The translational energy dependence is investigated under single-collision conditions using a guided-ion beam (GIB) apparatus. The GIB apparatus is equipped with a high-temperature octopole (HT8P) capable of studying reactions from 300 to 1100 K (±3% accuracy). A brief summary of each apparatus is given below.

The VT-SIFT instrument[30] consists of a remote, differentially-pumped electron impact ion source which directs ions into a quadrupole mass filter where the ionic species of interest is mass selected. Several methods are employed to eliminate electronic and vibrational excitation of the primary reactant ions. By introducing a flow of N_2 into the tube upstream of the reaction zone, vibrationally excited states of NO^+ and O_2^+ are quenched prior to reaction.[31] Furthermore, only excited electronic states of NO^+ and O_2^+ charge transfer with N_2,[14] so it is possible to monitor the formation of N_2^+ and then vary source conditions until less than 2% of the NO^+ and O_2^+ primary ions are electronically excited. The formation of the excited spin−orbit state of Xe^+ is reduced to <1% of the total Xe^+ by running with a small amount of N_2O in the source.[32] The ground spin−orbit states of Kr^+ ions are formed from the fragmentation of Kr_2^+ dimer ions upon injection into the flow tube.[30]

The mass-selected ions are injected into a fast flow of helium carrier gas in a meter long stainless steel flow tube. The apparatus is also equipped with a drift tube which allows the translational energy of the reactants to be varied up to approximately 0.5 eV collision energy. When operated in this drift mode, the apparatus is referred to as a selected ion flow drift tube (SIFDT). In both normal and drift modes, reactant hydrocarbon vapor is introduced into the flow tube and allowed to react over a known distance at a known flow velocity. A second mass spectrometer resolves the primary reactant and the secondary product ions which are then detected by an electron multiplier. The decay in the primary reactant ion signal as a function of increasing hydrocarbon vapor flow rate yields the reaction rate constant, and the product branching fractions are obtained by scanning the second mass spectrometer over the mass ranges of interest. The absolute uncertainties of the measurements are 25% and relative uncertainties are 15%.

The operation of the HTFA instrument[33,34] is similar to the VT-SIFT with the exception that there is no mass filter after the ion source. In the HTFA, ions are created by electron impact ionization and Penning ionization in a heated fast flow tube where the operating conditions are optimized for a single ionic species. Electronically and vibrationally excited states of NO^+ and O_2^+ are quenched prior to reaction by introducing a large flow of the source gas, NO and O_2, respectively, upstream of the reaction zone. Extensive fragmentation of the product organic is one indication that excited-state ions are present in the flow tube. Therefore, the product branching fractions are monitored as a function of source gas flow rate. The minimum flow rate is taken to be the flow rate at which the presence of excited-state primary ions impacts the branching fractions. The results presented here are taken with source gas flow rates in excess of 10 times the minimum value. In the NO^+ + ethylbenzene and *n*-propylbenzene experiments, the product charge-transfer ions reacted with the large excess of NO via hydrogen transfer to produce HNO. The hydrogen transfer rates at 500 K are slow (ca. 10^{-12}) and decrease rapidly with temperature. To correct for the NO secondary chemistry, the branching fractions have been measured at several NO flow rates and extrapolated back to zero NO concentration. The accuracy of this correction was confirmed by the excellent agreement between the 500 K corrected HTFA results obtained with a large excess of NO in the flow tube and SIFT data obtained with no excess NO in the flow tube. The absolute uncertainties of the measurements are 25% and relative uncertainties are 15%.

In the GIB instrument[35] with incorporated HT8P,[19,36] primary ions are generated by electron impact ionization in a continuous ion source that features magnetically confined electron beams. The primary ions are created in their ground electronic states by operating the ion source with an electron energy less than that required to reach the first long-lived excited state of the molecular ions. For NO^+ and O_2^+, electron energies of <15.5 and <16 eV are used, respectively. For these energies, electron impact ionization is expected to be subject to Franck−Condon factors which have been derived from photoelectron spectroscopy. Therefore, NO^+ and O_2^+ should have vibrational states up to $v = 4$ populated, with relative populations for $v = 0-4$ of approximately 1.0:2.2:1.9:1.1:0.5 and 1.0:2.0:2.1:1.0:0.2, respectively.[37]

The resulting ion beam is directed onto the main axis of the instrument by a 90° dc quadrupole bender, after which the beam is mass-selected using a Wien velocity filter. The primary ion beam is decelerated prior to being injected into the high-temperature octopole ion guide. The octopole guides the ions through a heated scattering cell containing the target vapor, and the resulting secondary ions and transmitted primary ions continue to the end of the ion guide where they are extracted into a quadrupole mass filter for analysis. The target gas temperature is measured using three thermocouples attached to the heated scattering cell. The heated octopole rods that pass through the cell aid in ensuring a uniform target gas temperature. The ions are detected using an off-axis channeltron. The ion beam kinetic energy, with a typical distribution of 0.25 eV full width at half-maximum, is established by adjusting the octopole dc potential and is measured to within ±0.05 eV by retarding potential and time-of-flight measurements. Monitoring the secondary and primary ion intensities as the ion beam energy is varied yields the reaction cross sections. Small differences in extraction efficiency of the primary and secondary ions due to differences in velocity are minimized by computer-controlled adjustment of the extraction lenses. The target gas density, measured with a capacitance manometer, is maintained in the 0.15−0.30 mTorr range where the effect of secondary collisions is minimized. To further ensure single-collision conditions, the guiding rf field is briefly turned off every 1 ms in order to purge secondary ions that are trapped by the octopole rod surface potential barriers. Thermal decomposition of target gas on the rod surfaces increases these surface barriers preventing operation of the high-temperature octopole at ion energies below 0.5 eV. The absolute error in the reported measurements is ±30%, while the relative error is ±15%.

In both the VT-SIFT and HTFA, the aromatic reactant enters the flow tube via a mass flow controller. In the case of *n*-propylbenzene, a bubbler system is employed where helium carrier gas passes through a sample of *n*-propylbenzene, becoming saturated with vapor. The flow rate of *n*-propylbenzene is derived from the known vapor pressure at room temperature along with the helium flow rate and the total pressure in the bubbler. Adjusting the helium flow and the total pressure varies the concentration of *n*-propylbenzene introduced into the reaction region.[38] In the GIB-HT8P apparatus, the target aromatic reactant is introduced into the collision cell using a variable leak valve.

Pure toluene (Aldrich, 99+%), ethylbenzene (Aldrich, 99+%), and *n*-propylbenzene (Aldrich, 98+%) reagents are used after several freeze−thaw cycles to remove trapped gases. The nitrogen and oxygen source gases used to create N_2^+, O_2^+, and O^+ ions are 99.999% pure (AGA). Other source gases employed are nitric oxide (Matheson, 99.3%), krypton (AGA, 99.999%), and xenon (Matheson, 99.999%). The helium buffer gas used in both flow tubes is 99.997% pure (AGA) and is passed through a liquid nitrogen cooled sieve trap to remove any water vapor.

III. Results

In Tables 1−7, the rate constants are listed in italics and are given in units of 10^{-9} cm^3 s^{-1}, the enthalpies of reaction, ΔH_{rxn}^{298}, are given in eV, assumed neutral products are given in parentheses, and estimated enthalpies are given in braces. The standard heats of formation used in the calculations are from Lias et al.[39] Table 1 shows the rate constants and product branching fractions for the reactions of toluene, ethylbenzene, and *n*-propylbenzene with NO^+, Xe_2^+, O_2^+, $Xe^+(^2P_{3/2})$, and $Kr^+(^2P_{3/2})$ measured at 300 and 500 K in the VT-SIFT (hereafter referred to as SIFT) apparatus. In the case of NO^+ and O_2^+, the SIFT results are compared to those of the GIB-HT8P (hereafter referred to as HT8P) at 300 K and to the HTFA at 500 K. The HT8P results correspond to the lowest CM translational energies observed which are in the 0.1−0.8 eV range. As noted in the Experiment section, the NO^+ and O_2^+ produced in the HT8P have average vibrational energies of 0.49 and 0.36 eV, respectively. Therefore, the HT8P experiments have more energy available for reaction than the flow tube experiments conducted at the same temperature. The average rovibrational energy of the aromatic reactant and the recombination energy of the primary ion are also shown in Table 1. The vibrational frequencies for toluene, ethylbenzene, and *n*-propylbenzene have been calculated for all normal modes using the Gaussian 98 program[40] at the HF/6-31G(d) level. The recombination energy for NO^+, O_2^+, $Xe^+(^2P_{3/2})$, and $Kr^+(^2P_{3/2})$ is simply the ionization energy of the neutral precursor. The recombination energy of Xe_2^+ corresponds to the vertical recombination energy to the repulsive region of the Xe_2 potential[41,42] and is calculated using the method of Praxmarer et al.[43]

Overall, the total reaction rate constants reported in Table 1 are large and are approximately equal to the thermal energy

TABLE 1: Reaction Rate Constants (10^{-9} cm^3 s^{-1}) and Product Branching Fractions for Ion−Alkylbenzene Reactions from 300 to 500 K Measured with the High-Temperature Octopole (HT8P), Selected Ion Flow Tube (SIFT), and High-Temperature Flowing Afterglow (HTFA)[a]

reaction (recombination energy)	products	ΔH^{298}_{rxn}, eV	HT8P[b] 300 K	SIFT 300 K	SIFT 500 K	HTFA 500 K
		Toluene				
av rovibrational energy (eV)			0.12	0.12	0.33	0.33
$NO^+ + C_7H_8 \rightarrow$	products			*1.6 [1.8]*	*1.9 [1.8]*	*2.0 [1.8]*
(9.26 eV)	$C_7H_8^+ + NO$	−0.44	1.00	1.00	1.00	1.00
$Xe_2^+ + C_7H_8 \rightarrow$	products			*1.3 [1.0]*		
(10.4 eV)	$C_7H_8^+ + 2Xe$	−1.58		1.00		
$O_2^+ + C_7H_8 \rightarrow$	products			*1.7 [1.8]*	*1.9 [1.7]*	*1.6 [1.7]*
(12.07 eV)	$C_7H_8^+ + O_2$	−3.25	0.58	1.00	0.88	0.85
	$C_7H_7^+ + H + O_2$	−1.54	0.42		0.12	0.15
$Xe^+ + C_7H_8 \rightarrow$	products			*1.3 [1.2]*		
(12.13 eV)	$C_7H_8^+ + Xe$	−3.31		0.87		
	$C_7H_7^+ + H + Xe$	−1.60		0.13		
$Kr^+ + C_7H_8 \rightarrow$	products			*1.3 [1.3]*		
(14.00 eV)	$C_7H_8^+ + Kr$	−5.18		0.08		
	$C_7H_7^+ + H + Kr$	−3.47		0.92		
		Ethylbenzene				
av rovibrational energy (eV)			0.14	0.14	0.40	0.40
$NO^+ + C_8H_{10} \rightarrow$	products			*2.0 [2.0]*	*1.7 [1.9]*	*1.6 [1.9]*
(9.26 eV)	$C_8H_{10}^+ + NO$	−0.50	0.96	1.0	0.97	0.96
	$C_8H_9^+ + (HNO)$	−0.86 }				0.01
	$+ (H + NO)$	1.30 }				
	$C_7H_7^+ + (CH_3NO)$	−1.04 }	0.04		0.03	0.03
	$+ (CH_3 + NO)$	0.73 }				
$Xe_2^+ + C_8H_{10} \rightarrow$	products			*1.4 [1.1]*		
(10.4 eV)	$C_8H_{10}^+ + 2Xe$	−1.64		0.91		
	$C_7H_7^+ + CH_3 + 2Xe$	−0.41		0.08		
	$C_6H_6^+ + C_2H_4 + 2Xe$	−0.05		0.01		
$O_2^+ + C_8H_{10} \rightarrow$	products			*2.2 [1.9]*	*2.2 [1.9]*	*1.6 [1.9]*
(12.07 eV)	$C_8H_{10}^+ + O_2$	−3.31	0.21	0.30	0.21	0.19
	$C_8H_9^+ + H + O_2$	−1.51			0.02	0.02
	$C_7H_7^+ + CH_3 + O_2$	−2.08	0.76	0.67	0.75	0.76
	$C_6H_6^+ + C_2H_4 + O_2$	−1.72	0.03	0.03	0.02	0.03
$Xe^+ + C_8H_{10} \rightarrow$	products			*1.5 [1.2]*		
(12.13 eV)	$C_8H_{10}^+ + Xe$	−3.37		0.18		
	$C_7H_7^+ + CH_3 + Xe$	−2.14		0.79		
	$C_6H_6^+ + C_2H_4 + Xe$	−1.78		0.03		
$Kr^+ + C_8H_{10} \rightarrow$	products			*1.4 [1.4]*		
(14.00 eV)	$C_8H_{10}^+ + Kr$	−5.24		0.07		
	$C_7H_7^+ + CH_3 + Kr$	−4.01		0.86		
	$C_6H_6^+ + C_2H_4 + Kr$	−3.65		0.07		
		n-Propylbenzene				
av rovibrational energy (eV)			0.17	0.17	0.48	0.48
$NO^+ + C_9H_{12} \rightarrow$	products			*2.1 [2.1]*	*2.1 [2.0]*	*2.1 [2.0]*
(9.26 eV)	$C_9H_{12}^+ + NO$	−0.55	0.98	1.00	1.00	1.00
	$C_7H_7^+ + C_2H_5 + NO$	0.67	0.02			
$Xe_2^+ + C_9H_{12} \rightarrow$	products			*1.4 [1.1]*		
(10.4 eV)	$C_9H_{12}^+ + 2Xe$	−1.69		0.95		
	$C_7H_7^+ + C_2H_5 + 2Xe$	−0.47		0.05		
$O_2^+ + C_9H_{12} \rightarrow$	products			*1.9 [2.0]*	*2.2 [2.0]*	*1.7 [2.0]*
(12.07 eV)	$C_9H_{12}^+ + O_2$	−3.36 }		0.18	0.12	0.11
	$C_9H_{11}^+ + H + O_2$	{−1.72} }	0.14			0.02
	$C_8H_9^+ + CH_3 + O_2$	−2.03	0.05	0.02	0.03	0.03
	$C_7H_8^+ + C_2H_4 + O_2$	−2.19 }		0.09	0.09	0.04
	$C_7H_7^+ + C_2H_5 + O_2$	−2.14 }	0.75	0.66	0.71	0.76
	$C_6H_6^+ + C_3H_6 + O_2$	−1.83	0.06	0.05	0.05	0.04
$Xe^+ + C_9H_{12} \rightarrow$	products			*1.4 [1.3]*		
(12.13 eV)	$C_9H_{12}^+ + Xe$	−3.42		0.04		
	$C_8H_9^+ + CH_3 + Xe$	−2.09		0.05		
	$C_7H_8^+ + C_2H_4 + Xe$	−4.12		0.06		
	$C_7H_7^+ + C_2H_5 + Xe$	−2.20		0.81		
	$C_6H_6^+ + C_3H_6 + Xe$	−1.89		0.04		

[a] The capture rate constant, k_c, is given in brackets next to the measured rate constants in italics. The enthalpies of reaction, ΔH^{298}_{rxn}, are given in eV for the assumed neutral products listed. Neutral products in parentheses and enthalpies in braces are estimated. [b] Corresponds to 0.4, 0.2, and 0.2 eV CM collision energy for toluene, ethylbenzene, and *n*-propylbenzene, respectively.

capture rate constants given by the Su−Chesnavich equation based on average dipole orientation theory,[44−46] appearing in brackets in the tables. The rate constants for Xe_2^+ appear to be supracollisional with rate constants approximately 30% above the capture rate constants and are outside of the reported error of the experiments. However, Xe_2^+ is distinguished from the

TABLE 2: Reaction Rate Constants (10^{-9} cm^3 s^{-1}) and Product Branching Fractions for the Reaction of NO^+ with Toluene from 650 to 1300 K Measured in the HTFA and the HT8P

reaction (recombination energy)	products	ΔH_{rxn}^{298}, eV	HT8P[a] 650 K	HTFA 900 K	HTFA 1050 K	HTFA 1100 K	HTFA 1300 K
av C_7H_8 rovibrational energy (eV)			0.55	1.03	1.35	1.47	1.95
$NO^+ + C_7H_8 \rightarrow$	products			*1.5 [1.8]*	*1.6 [1.8]*	*1.6 [1.8]*	*1.7 [1.8]*
(9.26 eV)	$C_7H_8^+ + NO$	−0.44	1.0	>0.99	0.93	0.80	0.28
	$C_7H_7^+ + (HNO)$	−0.90		<0.01	0.07	0.20	0.71
	$+ (H + NO)$	1.27					
	$C_6H_6^+ + (CH_2NO)$	0.98					0.01
	$C_6H_5^+ + (CH_3NO)$	0.07					

[a] Corresponds to 0.36 eV CM collision energy and ca. 0.49 eV of NO^+ vibrational energy (see text).

TABLE 3: Reaction Rate Constants (10^{-9} cm^3 s^{-1}) and Product Branching Fractions for the Reaction of O_2^+ with Toluene from 600 to 1200 K Measured in the HTFA and the HT8P

reaction (recombination energy)	products	ΔH_{rxn}^{298}, eV	HTFA 600 K	HT8P[a] 650 K	HTFA 800 K	HTFA 1000 K	HTFA 1200 K
av C_7H_8 rovibrational energy (eV)			0.47	0.55	0.83	1.24	1.71
$O_2^+ + C_7H_8 \rightarrow$	products		*2.0 [1.7]*		*1.7 [1.7]*		*1.9 [1.7]*
(12.07 eV)	$C_7H_8^+ + O_2$	−3.25	0.76	0.44	0.56	0.38	0.22
	$C_7H_7^+ + H + O_2$	−1.54	0.24	0.56	0.44	0.62	0.76
	$C_7H_6^+ + H_2 + O_2$	−0.67					0.02

[a] Corresponds to 0.74 eV CM collision energy and ca. 0.36 eV of O_2^+ vibrational energy (see text).

other primary ions studied here in that the ground electronic state of Xe_2 is repulsive. Such reactions are expected to be very efficient due to favorable Franck−Condon factors, perfect energy resonance conditions, and the irreversibility of dissociation. Supracollisional rate constants have also been observed for $O_2^+ + Na$ where a large number of dissociative O_2 electronic states are accessible.[36]

The reactions of NO^+ with the aromatic hydrocarbons listed in Table 1 produce charge-transfer products almost exclusively. This observation is consistent with the fact that fragmentation is endothermic in these cases. Increasing the recombination energy of the primary reactant ion produces more fragmentation as dissociative charge-transfer reaction channels become exothermic. The largest fraction of dissociative channels for all aromatic reactants proceeds through paths resulting in the production of the $C_7H_7^+$ ion. This result is consistent with previous mass spectrometric studies involving alkylbenzenes where the $C_7H_7^+$ ion is the most prominent fragment ion.[28,47−50] Two isomeric forms of the $C_7H_7^+$ ion can be formed in these reactions, the six-membered ring benzylium (Bz^+) cation and the seven-membered ring tropylium (Tr^+) cation. Note that the enthalpies of reaction in Tables 1−7 are calculated for the lower energy Tr^+ isomer which is 0.48 eV more stable than Bz^+. The isomers are distinguishable by their reactivity toward the parent aromatic compound.[51−53] In previous work relating to the reactivity of these alkylbenzenes at 300 K, the percentage of $C_7H_7^+$ in the Bz^+ isomeric form was found to remain fairly constant for each alkylbenzene over the recombination energy range of the experiments, indicating that the isomerization of Bz^+ to Tr^+ and vice versa is not an important factor.[27] The average percentage of $C_7H_7^+$ corresponding to the Bz^+ isomer was reported as follows: 55% for toluene; 67% for ethylbenzene; and 92% for *n*-propylbenzene. In the present experiments, the large partial pressures of the parent compound required to distinguish the two isomers could not be attained in the HTFA, so the Bz^+ to Tr^+ branching fraction has not been determined. Likewise, the HT8P experimental results do not distinguish between Bz^+ and Tr^+ isomers.

There is excellent agreement among the experimental results from the HT8P, SIFT, and HTFA in Table 1 with one exception. That is, the reaction of O_2^+ with toluene where 40% fragmentation is observed in the HT8P experiment and no fragmentation is observed in the flow tube studies at 300 K. In previous time-resolved photodissociation experiments of the toluene ion, the appearance energies to form Tr^+ and Bz^+ from toluene are observed to be very similar, 10.94 and 11.01 eV, respectively.[54] These energies are lower than the O_2^+ recombination energy. Spanel and Smith[55] also report only nondissociative charge-transfer products in their flow tube study of the O_2^+ reaction with toluene. There is an apparent shift in the flow tube dissociation threshold energy of at least 1 eV. Similar differences in flow tube dissociation thresholds have also been observed for benzene and naphthalene.[25,26] For benzene, the difference in threshold energies was attributed to the energized charge-transfer complex being collisionally stabilized by interactions with the He buffer.[25] The threshold energy shift for naphthalene was much larger and was attributed to a collisional stabilization effect and to a significant kinetic shift that results from the slow dissociation of the energized charge-transfer complex.[26]

Huang and Dunbar[56] have reported energy-dependent dissociation rates for the toluene cation, which allows the kinetic shift to be estimated. We anticipate a kinetic shift of approximately 0.6 eV in the flow tube experiments due to the slow dissociation rate of the toluene cation. Because the kinetic shift only partially explains the difference in threshold energies, we attribute the remainder to collisional stabilization of the energized charge-transfer complex by the He buffer, similar to what we have previously observed for benzene and naphthalene charge-transfer reactions in the flow tube.[25,26] The HT8P experiments show much more dissociation than the flow tube experiments. The fact that the HT8P experiments are conducted at a higher CM collision energy and that the O_2^+ primary reactant ion is vibrationally excited certainly contributes to the higher degree of fragmentation observed. However, the lower operating pressure may also contribute. The HT8P experiments are conducted at pressures under 10^{-4} Torr while the flow tube measurements are taken at 0.5 to 1 Torr. Therefore, the collisional stabilization of the energized charge transfer complex is not an issue in the HT8P experiments. Even in the absence of stabilizing collisions, the fragmentation observed in the HT8P is only 40%. The apparent incomplete dissociation may be

TABLE 4: Reaction Rate Constants (10^{-9} cm^3 s^{-1}) and Product Branching Fractions for the Reaction of NO^+ with Ethylbenzene from 650 to 900 K Measured in the HTFA and the HT8P

reaction (recombination energy)	products	ΔH^{298}_{rxn}, eV	HT8P[a] 650 K	HTFA 650 K	HT8P[a] 800 K	HTFA 800 K	HTFA 900 K
av C_8H_{10} rovibrational energy (eV)			0.67	0.67	1.00	1.00	1.25
$NO^+ + C_8H_{10} \rightarrow$	products			*1.5 [1.9]*		*1.9 [1.9]*	*2.0 [1.9]*
(9.26 eV)	$C_8H_{10}^+ + NO$	−0.50	0.96	0.96	0.88	0.71	0.25
	$C_8H_9^+ + (HNO)$	−0.86		0.01			0.02
	$+ (H + NO)$	1.30					
	$C_8H_8^+ + H_2 + NO$	0.39					0.01
	$C_7H_8^+ + (CH_2NO)$	0.41					0.01
	$+ (CH_2 + NO)$	3.81					
	$C_7H_7^+ + (CH_3NO)$	−1.04	0.04	0.03	0.12	0.29	0.71
	$+ (CH_3 + NO)$	0.73					

[a] Corresponds to 0.4 eV CM collision energy and ca. 0.49 eV of NO^+ vibrational energy (see text).

TABLE 5: Reaction Rate Constants (10^{-9} cm^3 s^{-1}) and Product Branching Fractions for the Reaction of O_2^+ with Ethylbenzene from 600 to 1000 K Measured in the HTFA and the HT8P

reaction (recombination energy)	products	ΔH^{298}_{rxn}, eV	HTFA 600 K	HT8P[a] 650 K	HTFA 700 K	HTFA 800 K	HTFA 1000 K
av C_8H_{10} rovibrational energy (eV)			0.57	0.67	0.78	1.00	1.51
$O_2^+ + C_8H_{10} \rightarrow$	products		*2.0 [1.9]*				*1.7 [1.9]*
(12.07 eV)	$C_8H_{10}^+ + O_2$	−3.31	0.16	0.15	0.14	0.08	0.02
	$C_8H_9^+ + H + O_2$	−1.51	0.02		0.02	0.02	0.03
	$C_8H_8^+ + H_2 + O_2$	−2.42					0.01
	$C_7H_7^+ + CH_3 + O_2$	−2.08	0.79	0.85	0.81	0.86	0.90
	$C_6H_6^+ + C_2H_4 + O_2$	−1.72	0.03		0.03	0.04	0.04
	$C_6H_5^+ + (C_2H_5 + O_2)$	−1.04					<0.01

[a] Corresponds to 0.77 eV CM collision energy and ca. 0.36 eV of O_2^+ vibrational energy (see text).

associated with long dissociation lifetimes and shorter observation times of approximately 200 μs in the HT8P experiment.

Tables 2−7 show the high-temperature results obtained in the HTFA and HT8P for reactions of NO^+ and O_2^+ with toluene, ethylbenzene, and *n*-propylbenzene. The reactions show a progression toward a greater extent of dissociative charge transfer (vs nondissociative) as the flow tube temperature increases. Rate constants have been measured at several temperatures over the ranges shown. In all cases, the rate constants attain values approximately equal to the capture rate constant. The thermal stability of the parent aromatic compound limited the maximum temperature reported. One indication of pyrolysis of the parent aromatic is the appearance of hydrogen-depleted ions not observed at lower temperatures in reactions with ions that have large recombination energies, i.e., N_2^+, Ne^+, and He^+, and produce a significant amount of fragmentation. For example, the appearance of $C_9H_9^+$, $C_9H_7^+$, $C_8H_8^+$, C_7H_6, $C_7H_5^+$, and $C_6H_4^+$ is a good indication that the aromatic reactant has partially decomposed, because these ions are most likely formed from the primary ions reacting with the hydrogen-depleted pyrolysis products of the aromatic reactant. Less than 2% of the total reactivity of toluene, ethylbenzene, and *n*-propylbenzene can be attributed to these product channels up to temperatures of 1300, 1000, and 900 K, respectively. Thermal decomposition data for these compounds under our experimental conditions, i.e., 1 Torr of He pressure and millisecond residence times, is limited, but the present results and relative stability of these aromatic species are consistent with the available data.[57−60]

In order to distinguish effects arising from adding energy to the reactants through ion recombination energy (electronic), temperature (rovibrational), and translational energy, breakdown diagrams for the aromatic charge transfer and $C_7H_7^+$ product branching fractions were constructed using the product distributions shown in Tables 1−7. Breakdown diagrams for toluene, ethylbenzene, and *n*-propylbenzene have been constructed and are shown in Figures 1−3, respectively. The relative abundances

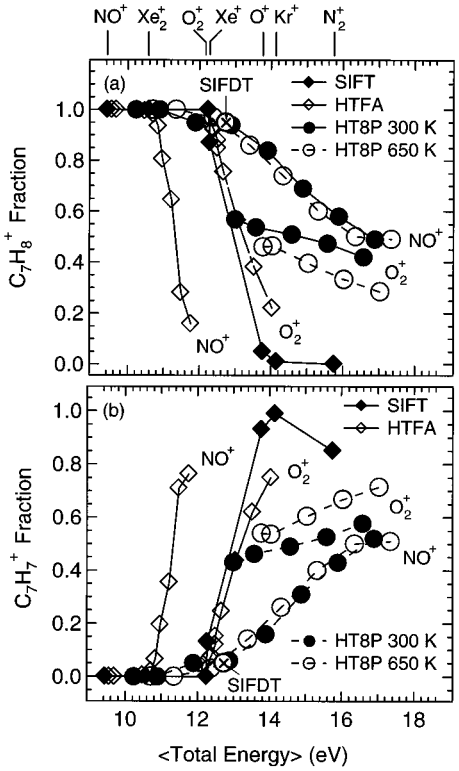

Figure 1. Breakdown diagrams for the reactions of toluene (C_7H_8) with various ions showing (a) $C_7H_8^+$ and (b) $C_7H_7^+$ as a function of average total energy. SIFT data corresponds to 300 K data of Table 1. HTFA data for NO^+ and O_2^+ reactions are recorded at temperatures above 300 K and include the data of Tables 2 and 3. HT8P data for NO^+ and O_2^+ reactions recorded at 300 and 650 K. An ⊗ symbol marks an O_2^+ SIFDT result corresponding to 300 K and a CM collision energy of 0.52 eV.

of the parent and $C_7H_7^+$ product ions are shown as a function of the average total reaction energy for each of the different

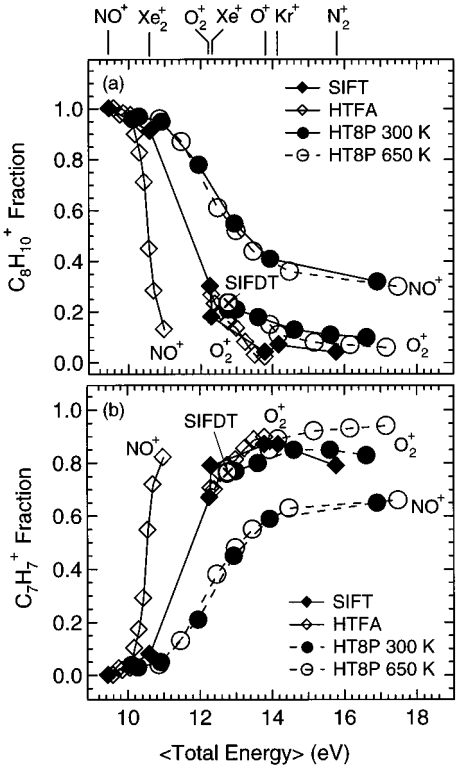

Figure 2. Breakdown diagrams for the reactions of ethylbenzene (C_8H_{10}) with various ions showing (a) $C_8H_{10}^+$ and (b) $C_7H_7^+$ as a function of average total energy. SIFT data corresponds to 300 K data of Table 1. HTFA data for NO^+ and O_2^+ reactions are recorded at temperatures above 300 K and include the data of Tables 4 and 5. HT8P data for NO^+ and O_2^+ reactions recorded at 300 and 650 K. An ⊗ symbol marks an O_2^+ SIFDT result corresponding to 300 K and a CM collision energy of 0.54 eV.

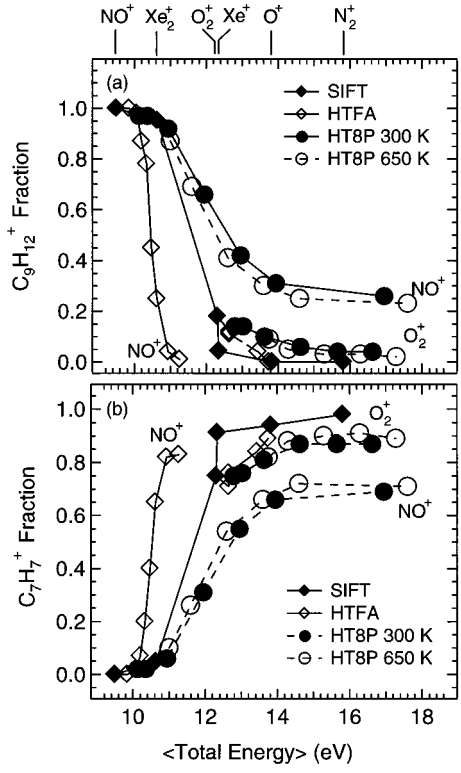

Figure 3. Breakdown diagrams for the reactions of *n*-propylbenzene (C_9H_{12}) with various ions showing (a) $C_9H_{12}^+$ and (b) $C_7H_7^+$ as a function of average total energy. SIFT data corresponds to 300 K data of Table 1. HTFA data for NO^+ and O_2^+ reactions are recorded at temperatures above 300 K and include the data of Tables 6 and 7. HT8P data for NO^+ and O_2^+ reactions recorded at 300 and 650 K.

experiments. The lines are an interpolation through the data and are meant to guide the eye. The minimum energy for each primary reactant ion studied corresponding to the 300 K SIFT data point is marked at the top of each figure. In Figures 1−3, the data labeled SIFT correspond to measurements taken at 300 K for each of the primary ions listed in Table 1 with the addition of the O^+ and N_2^+ SIFT data from our previous publication.[27] The HTFA data are represented by two sets of open diamonds corresponding to reactions of NO^+ and O_2^+ at temperatures above 300 K. Each HTFA data set originates at either the NO^+ or O_2^+ minimum energy point noted on the top of the figures. More temperatures have been studied in the HTFA experiments than are reported in Tables 2−7 and these additional data are plotted in the figures. The HT8P data for NO^+ or O_2^+ also originate at their respective minimum energy markers shown on the top of the figures.

The energy dependence of the branching fraction of the toluene charge-transfer product ($C_7H_8^+$) is shown in Figure 1a. For each set of data plotted in Figure 1a, the falloff in the $C_7H_8^+$ branching fraction is associated with a concomitant increase of the $C_7H_7^+$ product branching fraction as seen in Figure 1b. The data shown in Figure 1 exhibit a sharp falloff of the $C_7H_8^+$ branching fraction at an average total energy of approximately 12 eV with the NO^+ HTFA data being the exception. The NO^+ data fall off at approximately the thermodynamic threshold for formation of $C_7H_7^+$ at 10.5 eV. This fragmentation at lower total energies can be explained by the thermal decomposition of the $C_7H_8^+$ ion resulting from collisions with the helium buffer gas, i.e., $C_7H_8^+ + M \rightleftarrows C_7H_7^+ + H + M$, at temperatures greater than 1000 K. Similar behavior was observed for the iso-$C_8H_{17}^+$ ion produced in reactions of isooctane with NO^+.[20] The most convincing evidence supporting thermal decomposition via collisions with the buffer gas is the 300 K NO^+ HT8P data taken under single-collision conditions which do not exhibit significant fragmentation at total energies less than 12 eV. Furthermore, the SIFT data, taken at the same pressure as the HTFA but at a lower temperature, do not result in any significant fragmentation below a total energy of 12 eV. The $C_7H_7^+$ product ion resulting from the thermal decomposition appears to be stable up to temperatures as high as 1300 K under our conditions as indicated by the lack of a falloff of the $C_7H_7^+$ branching fraction in the HTFA data shown in Figure 1b.

Assuming that the fragmentation of the NO^+ HTFA data below 12 eV is due to thermal decomposition, the remaining data plotted in Figure 1 suggest that rovibrational energy is nearly as effective as electronic energy in promoting fragmentation and that both of these are much more effective than translational energy. The equivalence of electronic and rovibrational energy in promoting fragmentation follows from the fact that the O_2^+ HTFA and SIFT breakdown curves nearly overlap. Recall that at 300 K very little internal energy is available for reaction (Table 1), so that increasing the recombination energy of the primary reactant ion, as in the SIFT experiments, results in additional electronic energy being available for reaction. In the O_2^+ HTFA experiments, on the other hand, the recombination energy is held constant and the rovibrational energy is increased as shown in Table 3. Therefore, the nearly identical and rapid decrease in the $C_7H_8^+$ branching fraction with energy is indicative of the effectiveness of these types of energy in promoting dissociation. Because the NO^+ data suggest that $C_7H_8^+$ dissociates at temperatures above 1050 K, the last O_2^+ HTFA data point taken at 1200 K reflects some

TABLE 6: Reaction Rate Constants (10^{-9} cm^3 s^{-1}) and Product Branching Fractions for the Reaction of NO^+ with *n*-Propylbenzene from 650 to 900 K Measured in the HTFA and the HT8P

reaction (recombination energy)	products	ΔH^{298}_{rxn}, eV	HT8P[a] 650 K	HTFA 650 K	HT8P[a] 800 K	HTFA 800 K	HTFA 900 K
av C_9H_{12} rovibrational energy (eV)			0.80	0.80	1.19	1.19	1.48
$NO^+ + C_9H_{12} \rightarrow$	products			*2.3 [2.0]*		*2.1 [2.0]*	*2.1 [2.0]*
(9.26 eV)	$C_9H_{12}^+ + NO$	−0.55	0.87	0.86	0.82	0.21	0.04
	$C_9H_{11}^+ + (HNO)$	{−1.08}		0.06		0.04	
	$+ (H + NO)$	{1.09}					
	$C_9H_{10}^+ + H_2 + NO$	0.06				<0.01	0.01
	$C_8H_9^+ + (CH_3NO)$	−0.99		0.01		0.03	0.07
	$+ (CH_3 + NO)$	0.78					
	$C_7H_8^+ + C_2H_4 + NO$	0.62		0.01		0.05	0.05
	$C_7H_7^+ + (C_2H_5 + NO)$	0.67	0.10	0.07	0.18	0.65	0.82
	$C_6H_6^+ + C_3H_6 + NO$	0.98	0.02			0.01	0.01

[a] Corresponds to 0.40 eV CM collision energy and ca. 0.49 eV of NO^+ vibrational energy (see text).

TABLE 7: Reaction Rate Constants (10^{-9} cm^3 s^{-1}) and Product Branching Fractions for the Reaction of O_2^+ with *n*-Propylbenzene from 650 to 900 K Measured in the HTFA and the HT8P

reaction (recombination energy)	products	ΔH^{298}_{rxn}, eV	HT8P[a] 650 K	HTFA 650 K	HTFA 800 K	HTFA 900 K
av C_9H_{12} rovibrational energy (eV)			0.80	0.80	1.19	1.48
$O_2^+ + C_9H_{12} \rightarrow$	products			*1.7 [2.0]*		*1.7 [2.0]*
(12.07 eV)	$C_9H_{12}^+ + O_2$	−3.36		0.12	0.04	
	$C_9H_{11}^+ + H + O_2$	{−1.72}	0.09	0.01		0.01
	$C_9H_{10}^+ + H_2 + O_2$	−2.75				
	$C_9H_9^+ + H_2 + H + O_2$	{−0.71}				0.01
	$C_8H_9^+ + CH_3 + O_2$	−2.03	0.04	0.03	0.03	0.04
	$C_7H_8^+ + C_2H_4 + O_2$	−2.19	0.82	0.04	0.04	0.02
	$C_7H_7^+ + (C_2H_5 + O_2)$	−2.14		0.76	0.84	0.89
	$C_6H_6^+ + C_3H_6 + O_2$	−1.83	0.05	0.04	0.05	0.03

[a] Corresponds to 0.47 eV CM collision energy and ca. 0.36 eV of O_2^+ vibrational energy (see text).

thermal decomposition effects as well. Careful inspection of Figure 1 and Table 1 reveals that, although O_2^+ and Xe^+ have nearly identical energetics, toluene reacting with Xe^+ produces more fragmentation. A possible explanation is that the O_2 neutral formed in the reaction is electronically and/or vibrationally excited, thus leaving less energy available for excitation of the charge-transfer product ion. The first electronic state of O_2 is the a $^1\Delta_g$ state lying approximately 1 eV above the ground state.[61] If the reaction predominately forms O_2(a $^1\Delta_g$) product, then the observed dissociation threshold could be shifted by as much as 1 eV to higher energy. Furthermore, any rovibrational excitation would produce a shift to higher energy as well. The present experiment deals with energies that are averaged over Boltzmann distributions, and hence, the data points shown in the figures represent a range of energies. Therefore, given the limited energy resolution of the flow tube experiments, the formation of internally excited O_2 remains a possibility.

Both the recombination energy and rovibrational energy are held constant in the HT8P experiments, and the CM collision energy is increased independently. As shown in Figure 1a, the decrease in the $C_7H_8^+$ branching fraction with increasing average total energy is substantially more gradual for the HT8P data than in the flow tube studies, indicating that translational energy is less effective than electronic and rovibrational energy in promoting fragmentation. Note that translational energies well in excess of the dissociation threshold do not produce 100% fragmentation. In addition, the HT8P NO^+ and O_2^+ data at high average total energy level off at different $C_7H_8^+$ branching fractions, with the O_2^+ primary ion at 650 K producing the most fragmentation. The data suggest that the maximum degree of fragmentation at high translational energy is related to the amount of electronic and rovibrational energy available. To confirm that the differences observed between the HT8P and flow tube measurements are not artifacts of the different methods, an O_2^+ flow drift tube measurement (marked SIFDT) was made at a collision energy of 0.52 eV and is shown in Figure 1. As can be seen in the figure, the SIFDT data point is in good agreement with the translational energy dependence measured with the HT8P.

Parts a and b of Figure 2 show the breakdown curve for the ethylbenzene charge-transfer product ($C_8H_{10}^+$) and the branching fraction for the $C_7H_7^+$ fragment ion, respectively. Again, the NO^+ HTFA data fall off at approximately the thermodynamic threshold for formation of $C_7H_7^+$ at 10.0 eV. As observed in the NO^+ + toluene system, the dissociation onset observed in the SIFT and HT8P experiments occurs at higher energy than the thermodynamic threshold. Furthermore as shown in Table 4, the $C_8H_{10}^+$ branching fraction at 800 K for the HT8P experiment is significantly larger than for the HTFA experiments despite the fact that the NO^+ primary ion in the HT8P data has an additional 0.49 eV of internal energy available for reaction. These differences further support the supposition that thermal decomposition of the $C_8H_{10}^+$ ion occurs in the higher pressure HTFA experiment at temperatures above 700 K.

The O_2^+ HTFA and SIFT breakdown curves nearly overlap in Figure 2, suggesting that rovibrational energy is almost as effective as electronic energy in promoting fragmentation, and both of these are much more effective than translational energy. Note that the last three O_2^+ HTFA data points taken at temperatures above 700 K may reflect some thermal decomposition due to collisions with the helium buffer gas. As observed with toluene, reactions with Xe^+ produce more fragmentation than with nearly isoenergetic O_2^+, and the production of excited O_2 is also a possibility here. The difference between the low translational energy HT8P data and the flow tube data is much reduced compared to toluene. This improved agreement of the data suggests that the unimolecular dissociation rate of the excited $C_8H_{10}^+$ charge-transfer product ions has

increased compared to $C_7H_8^+$ because effects arising from kinetic shifts and collisional stabilization of the charge-transfer product are not as pronounced. This conclusion is supported by isotopic studies.[28] The dissociation products of deuterated toluene reactions are found to be statistically scrambled whereas the fragment ions produced from deuterated ethylbenzene are not, especially at high ion internal energies, indicating more rapid dissociation for ethylbenzene ions.

The reduced efficiency of translational energy in promoting dissociation is evidenced by the substantially more gradual decrease in the ethylbenzene charge-transfer branching fraction with increasing translational energy compared with electronic and rovibrational energy. Again, the SIFDT data point at a CM collision energy of 0.54 eV is in good agreement with the translational energy dependence exhibited by the HT8P data. As in the toluene reactions at high translational energies, the HT8P NO^+ and O_2^+ data level off at different $C_8H_{10}^+$ branching fractions with the 650 K O_2^+ data producing the most fragmentation. These results further support the idea that the maximum degree of fragmentation is related to the amount of electronic and rovibrational energy available. Translational energy appears to be more effective in promoting fragmentation in ethylbenzene reactions than for toluene. This statement follows from the fact that the amount of fragmentation produced by adding translational energy is larger for ethylbenzene than for toluene.

Data for *n*-propylbenzene reactions are shown in Figure 3. As for the previous two alkylbenzenes, the NO^+ HTFA data falls off at the energetic threshold for formation of $C_7H_7^+$ at 9.9 eV. This feature is similarly attributed to thermal decomposition of the *n*-propylbenzene charge-transfer product ($C_9H_{12}^+$) which begins at a temperature of approximately 625 K under our conditions. Because the O_2^+ and Xe^+ data produce so much fragmentation at 300 K, it is difficult to confirm the relative effectiveness of rovibrational and electronic energy in this reaction. However, the few data points in this region are consistent with the conclusion drawn regarding the toluene and ethylbenzene reactions that both forms of energy are equally effective in promoting fragmentation. The steep translational energy dependence and low asymptotic value of the $C_9H_{12}^+$ branching fraction, compared to toluene and ethylbenzene, indicate that translational energy is the most effective in the *n*-propylbenzene system for promoting fragmentation. Indeed, the NO^+ HT8P translational energy data have nearly the same energy dependence as the electronic energy data represented by the SIFT experiment. The similarity of the low translational energy HT8P and the flow tube data suggests that the unimolecular dissociation rate of the excited $C_9H_{12}^+$ charge-transfer product ions has increased compared to $C_8H_{10}^+$ and $C_7H_8^+$, i.e., kinetic and pressure (collisional stabilization of the charge-transfer product) shifts are the least apparent in the *n*-propylbenzene reactions. This conclusion is supported by the dissociation rate energy dependence for toluene[62] and propylbenzene.[50] For example, at a total energy of ca. 12.1 eV corresponding to reactions with O_2^+, the dissociation lifetime for $C_7H_8^+$ is approximately 20 μs whereas the dissociation lifetime for $C_9H_{12}^+$ is 0.1 μs.

IV. Discussion

The dynamics for gas-phase charge-transfer systems[29] can be categorized in three mechanisms: (1) *Complex formation* with efficient conversion of translational energy into internal energy through energy randomization. (2) Low-impact parameter, *hard-sphere type* collisions in which the charge-transfer product is vibrationally excited through repulsive interactions. This mechanism becomes significant if the radius associated with the representative hard-sphere cross section of the collision system is comparable to the average interfragment distance at which the electron hop occurs. (3) *Near-resonant charge transfer* governed by state-to-state charge-transfer probabilities where a transition occurs from predominantly vibrational coupling to primarily radial coupling as the collision energy is raised from thermal energies.[63] While the vibrationally coupled mechanism is governed to a large degree by adiabatic transitions involving curve crossings along vibrational coordinates, the radially coupled transitions encompass near-resonant Franck−Condon active product states, where the width of the product state distributions about resonance is governed by the nonadiabaticity of the interaction. The width and nonadiabaticity increase progressively with translational energy.

All of the reactions studied here proceed rapidly at approximately the thermal energy capture rate. The large reaction rate constants observed in these reactions are consistent with a complex formation mechanism. However, a predominance of the complex formation mechanism (mechanism 1) would express itself as an equivalence of electronic, rovibrational, and translational energy in promoting dissociative charge transfer. The flow drift tube (SIFDT) experiments shown in Figures 1 and 2 where approximately 0.5 eV of energy was put into translation did not produce as much fragmentation as the same amount of energy put into electronic (SIFT) or rovibrational (HTFA) energy. The HT8P data confirm this observation. This transational energy dependence suggests that complex formation is most significant at thermal and lower CM collision energies. Therefore, the reduced efficiency of translational energy observed in these reactions suggests that near-resonant charge transfer (mechanism 3) involving long-range interactions with minimal translational energy transfer plays a role at low translational energies.

Although the present work does not include a systematic measurement of absolute charge-transfer cross sections at hyperthermal energies, cross sections of $\sim$25 Å^2 are estimated for the NO^+ + *n*-propylbenzene system at translational energies above 2 eV. This relatively small cross section compared with the size of the target molecule is an indication that hard-sphere type collisions with repulsive interactions (mechanism 2) should play a significant role at hyperthermal energies for this particular collision system. Evidence for mechanism 2 is seen in the HT8P NO^+ + ethylbenzene and *n*-propylbenzene systems where the fragmentation branching fractions reflect threshold behavior similar to the line-of-centers functions observed in collision-induced dissociation (CID) experiments.[64] In CID experiments, the fragmentation cross section saturates at a value corresponding to an effective hard-sphere cross section. This saturation behavior resembles the flattening of the fragmentation branching fraction at high translational energies. However, as noted in the Results section, the maximum degree of fragmentation at high translational energy appears to be dependent on the initial energy available for reaction. For example, the amount of fragmentation observed for reactions of O_2^+ at high translational energies is greater than that observed for NO^+ which has a lower recombination energy. Indeed even the higher temperature O_2^+ HT8P data appears to yield more fragmentation than the lower internal energy 300 K data at high translational energies. These differences could reflect differences in the hard-sphere cross section. However, another possibility is that near-resonant charge transfer is occurring in addition to hard-sphere collisions at high translational energies resulting in an increase in fragmentation with increasing internal energy available.

Dissociation lifetimes in excess of the experimental time window of the beam experiment may substantially delay the observed onset of dissociation leading to a kinetic shift.[65] Dissociation lifetimes (~1 ms) associated with a tight transition state have been reported for unimolecular decay of excited toluene ions.[62] The observation of strong intramolecular benzene-to-alkyl charge-transfer transitions in photodissociation spectroscopic experiments of ethyl and *n*-propylbenzene ions, however, implies that the strong $\sigma-\pi$ interactions induced by the out-of-plane motion of the alkyl substituents result in a looser dissociation transition state, and hence an increased dissociation rate, for these ions.[28,50,62,66] This increased dissociation rate is consistent with the increase in apparent translational efficiency with the increasing size of the alkyl substituent. In addition, the approximately 1 eV kinetic and pressure shifts in the observed fragmentation thresholds for the SIFT and HTFA O_2^+ toluene data (Figure 1) appear to be much less pronounced for ethylbenzene data and even less for the *n*-propylbenzene results. Because kinetic and pressure shifts are dependent on the lifetime of the charge-transfer transition state, the threshold behavior is further evidence for an increased dissociation rate with increasing size of the alkyl substituent. Future studies including absolute cross section measurements, a recoil velocity analysis of charge-transfer and dissociative charge-transfer products, and an RRKM analysis of unimolecular dissociation times of ethyl and propylbenzene will provide more quantitative results.

V. Conclusions

Rate constants and product branching fractions have been measured for the reaction of several ions with toluene, ethylbenzene, and *n*-propylbenzene at temperatures ranging from 300 to 1400 K and CM collision energies ranging from 0.04 to 7 eV. The reactions proceed primarily by nondissociative and dissociative charge transfer except for the reactions involving NO^+, where the dissociation products observed in the HTFA experiments at high temperature are attributed to thermal decomposition of the charge-transfer product ions. The $C_7H_7^+$ ion is the dominant fragment ion observed for all three ion−alkylbenzene reaction systems over the energy ranges studied. Electronic and rovibrational energy are found to be nearly equivalent in promoting fragmentation whereas translational energy is found to be much less effective. The charge-transfer reactions involve several mechanisms whose relative importance depends heavily on the initial conditions of the reaction partners. At thermal CM collision energies, *complex formation* and *near-resonant charge transfer* are important. *Hard-sphere type collisions* are significant at the highest CM collision energies studied here (several electronvolts), but there is also supporting evidence for *near-resonant charge transfer* at these collision energies.

The ability to predict the behavior of complex reaction systems is particularly important for modeling applications which often require extrapolation of a limited amount of existing data to conditions of practical interest. Based on the present results which show essentially large, temperature-independent charge-transfer rate constants, the calculated Su−Chesnavich capture rate constant[44,45] is an excellent approximation for the total reaction rate constant for these ion−alkylbenzene reactions at any temperature. Furthermore, the breakdown curves shown in Figures 1−3 provide an excellent method for predicting the product branching fractions as a function of total energy for the alkylbenzene reactions studied here. The Bz^+ to Tr^+ branching ratio has not been determined at temperatures above 300 K. However, the present results suggest that the Bz^+ to Tr^+ branching ratio at high temperature could be estimated from the recombination energy dependence of the 300 K data based on the close similarity of the electronic and rovibrational energy dependence of the $C_7H_7^+$ product branching fractions.

Translational energy constitutes a small amount of the total energy available at a given temperature. However, if the reaction conditions are highly nonequilibrium and a disproportionate amount of the available energy is translational, as encountered in the GIB experiments, then the more complicated translational energy dependence needs to be considered. The data suggest that the maximum degree of fragmentation at high translational energy is related to the amount of electronic and rovibrational energy available. However, the relatively smooth translational energy dependence, coupled with the plateau observed in the branching fractions at high energy, should allow adequate approximations to be made to satisfy a variety of modeling applications. The results for toluene, and to some extent ethylbenzene and *n*-propylbenzene, suggest that the extent of observed dissociation will depend on the lifetime of the reaction complex, and therefore, on pressure. The present experiments do not address this important issue. However, experiments are planned to study the alkylbenzene reactions over a 1−760 Torr pressure range to provide the necessary information to fully transition these data for future detailed kinetic models.

Acknowledgment. We dedicate this article to Bradley Moore on the occasion of his 60th birthday. We thank John Williamson and Paul Mundis for technical support. A.J.M. is an Air Force Research Laboratory Scholar. This work was supported by AFOSR under Tasks 2303EP4 and 2303EP2.

References and Notes

(1) Harsha, P. T.; Edelman, R. B.; Farmer, R. C. "Fundamental Combustion Technology for Ramjet Applications"; Chemical Propulsion Information Agency Publication 363, 1982; Vol. II.

(2) Jachimowski, C. J. In *Major Research Topics in Combustion*; Hussaini, M. Y., Kumar, A., Voight, R. G., Eds.; Springer-Verlag: New York, 1991; p 339.

(3) Kay, I. W.; Peschke, W. T.; Guile, R. N. *J. Propul. Power* **1992**, *8*, 507.

(4) Hueter, U. Creating an airline to the stars. In *Aerospace America* **1999**, *37*, 40.

(5) Weinberg, F. J.; Horn, K.; Oppenheim, A. K. *Nature* **1978**, *271*, 341.

(6) Orrin, J. E.; Vince, I. M.; Weinberg, F. J. *Eighteenth Symposium (International) on Combustion, [Proceedings]*; The Combustion Institute: Pittsburgh, PA, 1981; p 1755.

(7) Henderson, R. E. AGARD Report R-824, NATO, 1997.

(8) Nagashima, T.; Kitamuar, H.; Obata, S. *Proc. XIII Int. Symp. Air Breathing Engines (ISABE), Chattanooga, TN* **1997**, 366.

(9) Mathur, T.; Streby, G.; Gruber, M.; Jackson, K.; Donbar, J.; Donaldson, W.; Jackson, T.; Smith, C.; Billig, F. Supersonic Combustion Experiments with a Cavity-Based Fuel Injector; AIAA 99-2102, 35th AIAA/ASME/SAE/ASEE Joint Propulsion Conference and Exhibit, Los Angeles, CA, 1999.

(10) Gruber, M. R.; Baurle, R. A.; Mathur, T.; Hsu, K.-Y. Fundamental Studies of Cavity-Based Flameholder Concepts for Supersonic Combustors; AIAA 99-2248, 35th AIAA/ASME/SAE/ASEE Joint Propulsion Conference and Exhibit, Los Angeles, CA,1999.

(11) Calcote, H. F.; Gill, R. J. In *Comparison of the Ionic Mechanism of Soot Formation with a Free Radical Mechanism*; Bockhorn, H., Ed.; Springer-Verlag: Heidelberg, Germany, 1994; p 471.

(12) *Ionization in High-Temperature Gases*; Shuler, K. E., Fenn, J. B., Eds.; Academic Press: New York, 1962; Vol. 12.

(13) *Advanced Combustion Methods*; Weinberg, F. J., Ed.; Academic Press: London, 1986.

(14) Ikezoe, Y.; Matsuoka, S.; Takebe, M.; Viggiano, A. A. *Gas-Phase Ion−Molecule Reaction Rate Constants Through 1986*; Maruzen Co., Ltd.: Tokyo, 1987.

(15) Lindinger, W.; Fehsenfeld, F. C.; Schmeltekopf, A. L.; Ferguson, E. E. *J. Geophys. Res.* **1974**, *79*, 4753.

(16) Chen, A.; Johnsen, R.; Biondi, M. A. *J. Chem. Phys.* **1978**, *69*, 2688.

(17) Viggiano, A. A.; Dotan, I.; Morris, R. A. *J. Am. Chem. Soc.* **2000**, *122*, 353.
(18) Hierl, P. M.; Friedman, J. F.; Miller, T. M.; Dotan, I.; Mendendez-Barreto, M.; Seeley, J.; Williamson, J. S.; Dale, F.; Mundis, P. L.; Morris, R. A.; Paulson, J. F.; Viggiano, A. A. *Rev. Sci. Instrum.* **1996**, *67*, 2142.
(19) Levandier, D. J.; Dressler, R. A.; Murad, E. *Rev. Sci. Instrum.* **1997**, *68*, 64.
(20) Arnold, S. T.; Viggiano, A. A.; Morris, R. A. *J. Phys. Chem. A* **1997**, *101*, 9351.
(21) Arnold, S. T.; Morris, R. A.; Viggiano, A. A. *J. Phys. Chem. A* **1998**, *102*, 1345.
(22) Arnold, S. T.; Viggiano, A. A.; Morris, R. A. *J. Phys. Chem. A* **1998**, *102*, 8881.
(23) Williams, S.; Arnold, S. T.; Bench, P. M.; Viggiano, A. A.; Dotan, I.; Midey, A. J.; Morris, T.; Morris, R. A.; Maurice, L. Q.; Sutton, E. A. Potential Enhancement of Hydrocarbon Fueled Combustor Performance via Ionization; ISABE 99-7236, 14th International Symposium on Air Breathing Engines, Florence, Italy, 1999.
(24) Williams, S.; Midey, A. J.; Arnold, S. T.; Bench, P. M.; Viggiano, A. A.; Morris, R. A.; Maurice, L. Q.; Carter, C. D. Progress on the Investigation of the Effects of Ionization on Hydrocarbon/Air Combustion Chemistry; AIAA 99-4907, 9th International Space Planes and Hypersonic Systems and Technologies Conference, Norfolk, VA, 1999.
(25) Arnold, S. T.; Williams, S.; Dotan, I.; Midey, A. J.; Morris, R. A.; Viggiano, A. A. *J. Phys. Chem. A* **1999**, *103*, 8421.
(26) Midey, A. J.; Williams, S.; Arnold, S. T.; Dotan, I.; Morris, R. A.; Viggiano, A. A. *Int. J. Mass Spectrom.* **2000**, *195*, 327.
(27) Arnold, S. T.; Dotan, I.; Williams, S.; Viggiano, A. A.; Morris, R. A. *J. Phys. Chem. A* **2000**, *104*, 928.
(28) Ausloos, P. *J. Am. Chem. Soc.* **1982**, *104*, 5259.
(29) Dressler, R. A.; Levandier, D. J.; Williams, S.; Murad, E. *Comments At. Mol. Phys.* **1998**, *34*, 43.
(30) Viggiano, A. A.; Morris, R. A.; Dale, F.; Paulson, J. F.; Giles, K.; Smith, D.; Su, T. *J. Chem. Phys.* **1990**, *93*, 1149.
(31) Ferguson, E. E. *J. Phys. Chem.* **1986**, *90*, 731.
(32) Adams, N. G.; Smith, D.; Alge, E. *J. Phys. B: Atom. Mol. Phys.* **1980**, *13*, 3235.
(33) Miller, T. M.; Friedman, J. F.; Menendez-Barreto, M.; Viggiano, A. A.; Morris, R. A.; Miller, A. E. S.; Paulson, J. F. *Phys. Scr.* **1994**, *T53*, 84.
(34) Hierl, P. M.; Dotan, I.; Seeley, J. V.; Van Doren, J. M.; Morris, R. A.; Viggiano, A. A. *J. Chem. Phys.* **1997**, *106*, 3540.
(35) Dressler, R. A.; Salter, R. H.; Murad, E. *J. Chem. Phys.* **1993**, *99*, 1159.
(36) Levandier, D. J.; Dressler, R. A.; Williams, S.; Murad, E. *J. Chem. Soc., Faraday Trans.* **1997**, *93*, 2611.
(37) Turner, D. W.; Baker, C.; Baker, A. D.; Brundle, C. R. *Molecular Photoelectron Spectroscopy*; Wiley-Interscience: London, 1970.
(38) Viggiano, A. A.; Perry, R. A.; Albritton, D. L.; Ferguson, E. E.; Fehsenfeld, F. C. *J. Geophys. Res.* **1980**, *85*, 4551.
(39) Lias, S. G.; Bartmess, J. E.; Liebman, J. F.; Holmes, J. L.; Levin, R. D.; Mallard, W. G. Ion Energetics Data. In *NIST Chemistry WebBook, NIST Standard Reference Database Number 69*; Mallard, W. G., Linstrom, P. J., Eds.; NIST: Gaithersburg, MD, 1998 (http://webbook.nist.gov).
(40) Frisch, M. J.; Trucks, G. W.; Schlegel, H. B.; Scuseria, G. E.; Robb, M. A.; Cheeseman, J. R.; Zakrzewski, V. G.; Montgomery, J. J. A.; Stratmann, R. E.; Burant, J. C.; Dapprich, S.; Millam, J. M.; Daniels, A. D.; Kudin, K. N.; Strain, M. C.; Farkas, O.; Tomasi, J.; Barone, V.; Cossi, M.; Cammi, R.; Mennucci, B.; Pomelli, C.; Adamo, C.; Clifford, S.; Ochterski, J.; Petersson, G. A.; Ayala, P. Y.; Cui, Q.; Morokuma, K.; Malick, D. K.; Rabuck, A. D.; Raghavachari, K.; Foresman, J. B.; Cioslowski, J.; Ortiz, J. V.; Stefanov, B. B.; Liu, G.; Liashenko, A.; Piskorz, P.; Komaromi, I.; Gomperts, R.; Martin, R. L.; Fox, D. J.; Keith, T.; Al-Laham, M. A.; Peng, C. Y.; Nanayakkara, A.; Gonzalez, C.; Challacombe, M.; Gill, P. M. W.; Johnson, B.; Chen, W.; Wong, M. W.; Andres, J. L.; Gonzalez, C.; Head-Gordon, M.; Replogle, E. S.; Pople, J. A., *Gaussian 98*; Gaussian, Inc.: Pittsburgh, PA, 1998.
(41) Barker, J. A.; Watts, R. O.; Lee, J. K.; Schafer, T. P.; Lee, Y. T. *J. Chem. Phys.* **1974**, *61*, 3081.
(42) Chen, E. C. M.; Dojahn, J. G.; Wentworth, W. E. *J. Phys. Chem.* **1997**, *101*, 3088.
(43) Praxmarer, C.; Hansel, A.; Lindinger, W.; Herman, Z. *J. Chem. Phys.* **1998**, *109*, 4246.
(44) Su, T.; Chesnavich, W. J. *J. Chem. Phys.* **1982**, *76*, 5183.
(45) Su, T. *J. Chem. Phys.* **1988**, *89*, 5355.
(46) Su, T.; Bowers, M. T. Classical Ion−Molecule Collision Theory. In *Gas Phase Ion Chemistry*; Bowers, M. T., Ed.; Academic Press: New York, 1979; Vol. 1, p 83.
(47) Lifshitz, C.; Malinovich, Y. *Int. J. Mass Spectrom. Ion Processes* **1984**, *60*, 99.
(48) Baer, T.; Dutuit, O.; Mestdagh, H.; Rolando, C. *J. Phys. Chem.* **1988**, *92*, 5674.
(49) Kuck, D. *Mass Spectrom. Rev.* **1990**, *9*, 187.
(50) Hwang, W. G.; Moon, J. H.; Choe, J. C.; Kim, M. S. *J. Phys. Chem. A* **1998**, *102*, 7512.
(51) Jackson, J. A.; Lias, S. G.; Ausloos, P. *J. Am. Chem. Soc.* **1977**, *99*, 7515.
(52) Dunbar, R. C. *J. Am. Chem. Soc.* **1975**, *97*, 1382.
(53) Shen, J.; Dunbar, R. C.; Olah, G. A. *J. Am. Chem. Soc.* **1974**, *96*, 6227.
(54) Lifshitz, C. *Acc. Chem. Res.* **1994**, *27*, 138.
(55) Spanel, P.; Smith, D. *Int. J. Mass Spectrom.* **1998**, *181*, 1.
(56) Huang, F.-S.; Dunbar, R. D. *J. Am. Chem. Soc.* **1990**, *112*, 8167.
(57) Braekman-Danheux, C.; Delaunois, C.; Quyen, N. C. *Fuel Process. Technol.* **1977**, *1*, 57.
(58) Bruinsma, O. S. L.; Moulijn, J. A. *Fuel Process. Technol.* **1988**, *18*, 213.
(59) Chen, Q.; Froment, G. F. *J. Anal. Appl. Pyrolysis* **1991**, *21*, 51.
(60) Li, Z.; Anderson, S. L. *J. Phys. Chem. A* **1998**, *102*, 9202.
(61) Herzberg, G. *Molecular Spectra and Molecular Structure: I. Spectra of Diatomic Molecules*; D. Van Nostrand Co., Inc.: New York, 1950.
(62) Huang, F.-S.; Dunbar, R. S. *Int. J. Mass Spectrom. Ion Processes* **1991**, *109*, 151.
(63) Dressler, R. A.; Arnold, S. T.; Murad, E. *J. Chem. Phys.* **1995**, *103*, 9989.
(64) Levine, R. D.; Bernstein, R. B. *Molecular Reaction Dynamics and Chemical Reactivity*; Oxford University Press: New York, 1987.
(65) Rogers, M. T.; Ervin, K. M.; Armentrout, P. B. *J. Chem. Phys.* **1997**, *106*, 4499.
(66) Dunbar, R. C. *J. Phys. Chem.* **1979**, *83*, 2376.